Molecular Crystals and Liquid Crystals
Publication details, including instructions for authors and subscription information:
http://www.tandfonline.com/loi/gmcl20

Charge Carrier Mobility and Ageing of ZnPc/C60 Solar Cells

V. Kažukauskas [a], A. Arlauskas [a], M. Pranaitis [a], R. Lessmann [b], M. Riede [b] & K. Leo [b]

[a] Department of Semiconductor Physics and Institute of Applied Research of Vilnius University, Vilnius, Lithuania

[b] Institut für Angewandte Photophysik, Technische Universität Dresden, Dresden, Germany

Version of record first published: 28 May 2010

To cite this article: V. Kažukauskas, A. Arlauskas, M. Pranaitis, R. Lessmann, M. Riede & K. Leo (2010): Charge Carrier Mobility and Ageing of ZnPc/C60 Solar Cells, Molecular Crystals and Liquid Crystals, 522:1, 61/[361]-74/[374]

To link to this article: http://dx.doi.org/10.1080/15421401003724175

Mol. Cryst. Liq. Cryst., Vol. 522: pp. 61/[361]–74/[374], 2010

ISSN: 1542-1406 print/1563-5287 online
DOI: 10.1080/15421401003724175

Taylor & Francis
Taylor & Francis Group

Charge Carrier Mobility and Ageing of ZnPc/C60 Solar Cells

V. KAŽUKAUSKAS,[1] A. ARLAUSKAS,[1]
M. PRANAITIS,[1] R. LESSMANN,[2] M. RIEDE,[2]
AND K. LEO[2]

[1]Department of Semiconductor Physics and Institute of Applied Research of Vilnius University, Vilnius, Lithuania
[2]Institut für Angewandte Photophysik, Technische Universität Dresden, Dresden, Germany

Cu and Zn Phtalocyanines (CuPc and ZnPc), and C60 are materials frequently used for organic Solar cell engineering. Their energy levels form a donor-acceptor junction, and they have high absorption coefficients and a complementary absorption for the Sun spectrum. We have investigated ageing properties of ZnPc/C60 Solar cells as they are influenced by the charge carrier mobility and variation of the potential barrier height of the ZnPc/C60 interface. The structures ITO/ZnPc/C60/C60:AOB/Al with a reasonable energy conversion efficiency of ~1.5% were investigated. The samples were aged for 1300 hours upon illumination with blue LED, with peak emission at 475 nm, and incident light power density of 10 mW/cm^2. The aged devices showed a strong and fast degradation of the short circuit current and of the fill factor after several hours followed by an almost constant behaviour of these values. The reference samples kept in the dark at the room temperature did show only very small changes in their I-V curves. Carrier mobility dependencies on electric field strength at different temperatures were measured by the Charge Extraction by Linearly Increasing Voltage (CELIV) method. It was demonstrated that mobility values decrease during degradation as compared to the reference samples. Nevertheless only mobility changes cannot explain the observed drop of device current. The increase of the effective barrier height at the interface of ZnPc and C60 by about 0.1 eV from ~0.55 eV up to ~0.65 eV was observed in the aged samples. Meanwhile thermal activation energy values of the electrical conductivity grew from about 0.28 eV prior to degradation up to about 0.34 eV after ageing.

Keywords CELIV; conductivity; fullerene; mobility; potential barrier height; solar cell; Zn phtalocyanines

PACS 42.70.Jk; 71.20.Rv; 72.20.Fr; 72.20.Jv; 73.40.Cg; 84.60.Jt

Address correspondence to V. Kažukauskas, Department of Semiconductor Physics and Institute of Applied Research, Vilnius University, Saulėtekio 9, bldg. 3, LT-10222 Vilnius, Lithuania. E-mail: vaidotas.kazukauskas@ff.vu.lt

1. Introduction

Organic solar cells based on small molecules are known to have reasonably high efficiencies since Tang introduced the heterojunction solar cell [1]. The excited states in organic semiconductors are usually excitons that have a high binding energy of more than 0.3 eV, thus they cannot be separated by thermal activation. The heterojunction between two semiconductors where one is an acceptor and another one is a donor is necessary to separate the excited states into positive and negative charge carriers.

Usually such type of conventional investigated heterojunctions include Phthalocyanines (Pc) and PTCDA [1], Phthalocyanines and C60 [2], and others. C60 is used in most cases as electron acceptor, its LUMO is located at around 3.9 eV [3]; it has a relatively high electron mobility up to $\sim 1\,cm^2/Vs$ (neat layer, [4]). The heterojunction formed between C60 and CuPc or ZnPc can separate excitons formed in both materials. The HOMO of ZnPc is located around 5.1 eV. This kind of solar cell can supply an open circuit voltage (V_{OC}) of about 0.5–0.6 V, a short circuit current density (I_{SC}) of about ten milliampere per square centimetre and a fill factor (FF) of above 0.5–0.6, leading to an energy conversion efficiency about 3% [5]. Other material combinations and/or tandem solar cells [6] yield even higher efficiencies reaching 5–6% [7,8], showing potential for more. Yet, the lifetime of high efficiency organic solar cells is still in the range of 1000 h, too low for most real applications. This is mainly attributed to contamination with oxygen and moisture that can react with excited molecules. From the research of OLEDs one can infer, that, in principle, organic molecules are very stable if not in contact with reactive species.

In the present work we have analysed the ageing and associated electrical properties (conductivity, the effective electron mobility, and energy parameters of material and interface) of the devices of ITO/ZnPc(18 nm)/C60(52 nm)/AOB (2%) doped C60(5 nm)/Al(100 nm). This device structure is chosen because it uses well-known materials that are stable at higher temperatures. A ZnPc buffer was used instead of the usual phenanthroline derivatives due to its higher thermal stability, without affecting the overall device behaviour.

2. Experimental

2.1. *Device Fabrication*

Devices were fabricated on and cut from a single larger glass plate called wafer. It contains 36 samples, arranged into 6 rows and 6 columns. The glass with patterned ITO layer is provided by TFD (Thin Film Devices, Inc). Before going into the glovebox, the wafer was cleaned in ultra sonic bath for 10 minutes each, in: ethanol, acetone, isopropanol. The substrate was further heated to 150°C in low vacuum in the load chamber of the glovebox for about 1 h. All organic and metal layers were deposited in the vacuum chamber without breaking the vacuum.

Chemical structures of the active materials are presented in Figure 1. Organic layers were deposited at a rate of 0.5 Å/s at a pressure below 5×10^{-6} Pa, and Al was evaporated at 15 Å/s at a pressure below 10^{-4} Pa. The organic dopant was deposited at a rate of 0.02 Å/s. The thicknesses of the layers were measured with independent calibrated quartz crystal monitors (QCM). The encapsulation was done on the wafer with a glass cover that has a cavity with a getter inside. The cover is glued to the glass substrate with a light curing sealant XNR5516 (Nagase GmbH). The encapsulation is performed in the nitrogen flooded glove box. After encapsulation

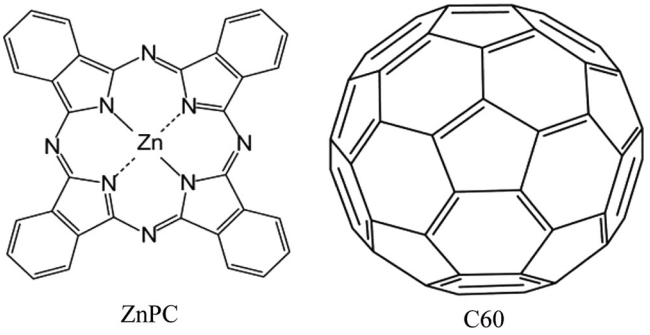

Figure 1. Chemical structures of the active materials ZnPC (left) and C60 (right).

the wafer was cut into the samples that were further stored in a glove box until they were characterized.

In the present work we have analysed the device structures consisting of ITO/ZnPc(18 nm)/C60(52 nm)/AOB(2%) doped C60(5 nm)/Al(100 nm). A ZnPc buffer was used instead of the usual phenanthroline derivatives due to its higher thermal stability, without affecting the overall device behaviour. The schematic layout of the sample cross section is presented in Figure 2. This structure is chosen because it utilises well-known materials that are stable at higher temperatures. Another more sophisticated test structure was used to improve barrier structure of the whole device: ITO/Au(1)/NDP2(1)/ZnPc(18 nm)/C60(52 nm)/AOB (2%) doped C60(5 nm)/Al(100 nm). NDP2 is a commercial strong organic acceptor, its electrical properties are to some extent similar to F4TCNq. Two different detector structures were fabricated on the same glass plate. In Figure 3 I-V curves in the dark and upon illumination by the blue LED of both structures are compared. It can be seen that indeed better carrier flow over the improved device is assured. Both kinds of devices had demonstrated the fill factor of about 42–45%, I_{SC} of the improved structure being higher, that was nevertheless accompanied by the decreased V_{OC}. Moreover, the notable differences in the IV shapes are visible at lower forward voltages. Nevertheless, these differences were not reflected by the mobility behaviour. Therefore further on we will analyse the conventional samples of the first type.

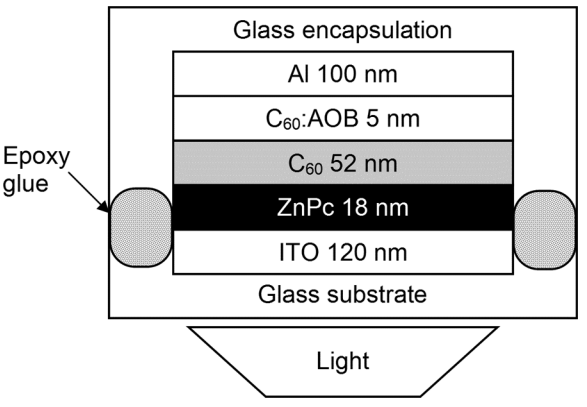

Figure 2. Schematic representation of the sample cross section.

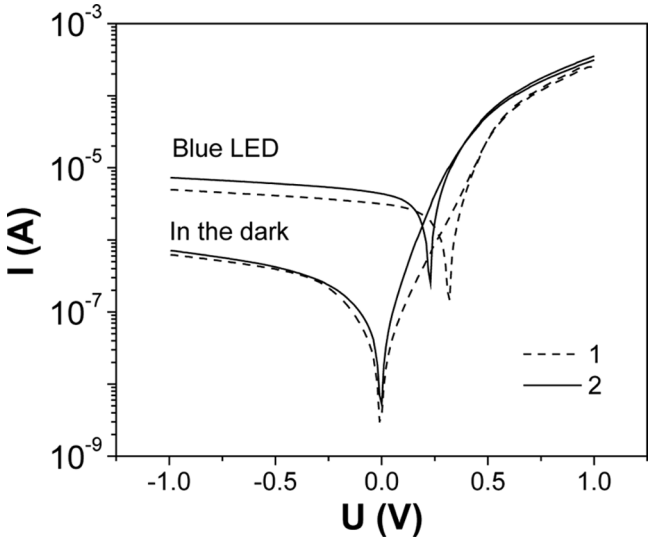

Figure 3. IV curves in the dark and upon illumination by the blue LED of two devices fabricated on the same glass plate with different structures: (1) ITO/ZnPc/C60/C60:AOB/Al (dashed curves) and (2) ITO/Au/NDP2/ZnPc/C60/C60:AOB/Al (solid curves).

2.2. *Experimental Setup*

A circuitry was developed to provide a stable illumination source, temperature control and a relay switcher to address all devices on one sample. The measurements of the current-voltage (IV) characteristics and their dependencies on time upon ageing was carried out by source-measure units Keithley 2400 and Keithley 6517A.

The light sources used for all long-time experiments were 1 W LXHL-PB01 Blue LED (nominal emission peak at 470 nm). The emission peak corresponds to an absorption peak of the C60 in the device structure (Fig. 4). The power of the LEDs (10 mW/cm^2) was measured with a calibrated photometer (Thorlabs PM100), and a metal mask to define the illuminated area. The LEDs have a junction to case thermal resistance of 15°C/W. Providing an active cooling of the LEDs it was possible to have no significant degradation of the Blue LEDs during the measurements.

To measure carrier mobility the original Charge Extraction by Linearly Increasing Voltage (CELIV) method was used, the detailed description of which is given in Ref. [9]. In CELIV, carrier extraction from the sample is assured by applying a triangular voltage pulse with a constant increase rate. To extract carriers at least one of the contacts should be blocking and voltage of the reverse polarity should be applied. The obtained CELIV traces, as, e.g., presented in Figure 5, demonstrate characteristic maxima, when the electric field in the sample becomes strong enough to extract most of the carriers. From these traces mobility can be calculated as:

$$\mu = \frac{2d^2}{3At_{\max}^2\left[1 + 0.36\frac{\Delta j}{j(0)}\right]}, \tag{1}$$

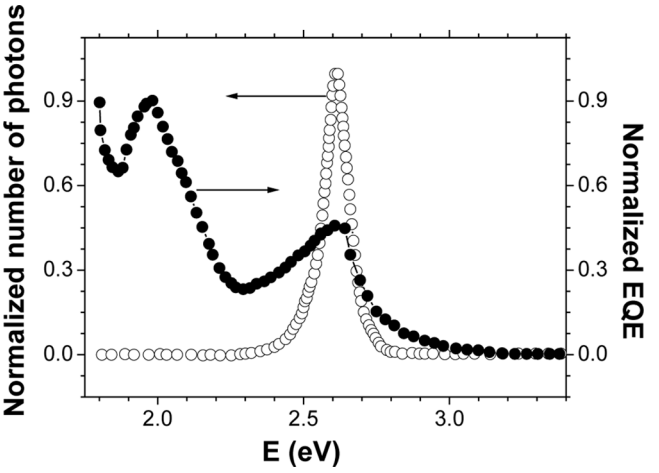

Figure 4. The comparative External Quantum Efficiency spectra of the investigated ZnPC/C60 devices and that of the light of the used blue LED.

and sample conductivity can be found as:

$$\sigma = \frac{3\varepsilon\varepsilon_0\Delta j}{2t_{\max}j(0)}. \tag{2}$$

Here A is the voltage increase rate, $t_{\max}$ is the time elapsed after the onset of the pulse, when characteristic maximum is observed, d is the sample thickness, $j(0)$ is the plateau value corresponding to the capacitive displacement current of the sample and Δj is the height of the current spike. In Eq. (1) the electric field re-distribution effect during charge extraction is taken into account. This makes mobility measurements in

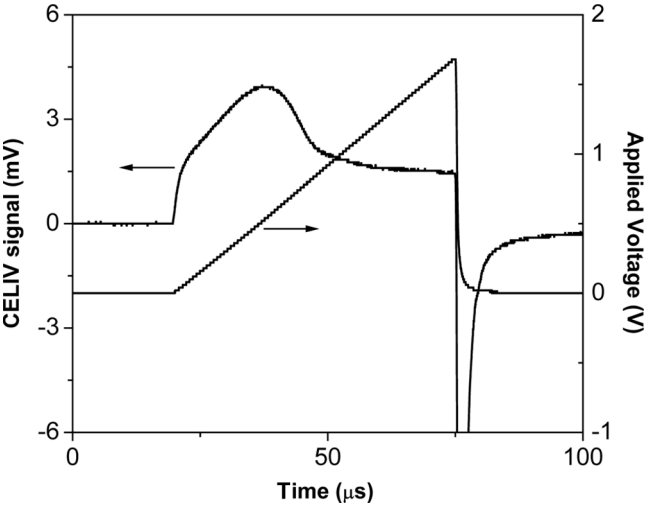

Figure 5. Example of the CELIV trace, demonstrating the characteristic maximum and the applied triangular voltage pulse.

conductive samples with relatively high carrier concentrations more reliable as compared to conventional Time-Of-Flight experiments. The classical TOF mobility measurement method [10] was many times proved to have sensitivity problems in dispersive materials. Moreover, it faces the fundamental limitations in high conductivity materials, originating from the requirement that dielectric relaxation time τ_σ must be longer than carrier transit time $t_{\rm tr}$. Only if this condition is fulfilled electric field in a sample remains constant over the sample thickness (otherwise it can be redistributed by equilibrium charge carriers in time intervals shorter that $t_{\rm tr}$), and carrier number does not decrease during their transit through the sample because of recombination. It was demonstrated in [11] that ignoring this fundamental limitation may cause an erroneous overestimation of the mobility values measured by TOF.

3. Results and Discussion

3.1. *Effect of Ageing on Cell Parameters*

The samples were aged for 1269 h, illuminated by a blue LED, with peak emission at 475 nm and incident light power density of $10\,\mathrm{mW/cm^2}$. The devices were encapsulated. The measurements of the current-voltage (I-V) characteristics and their dependencies on temperature and time upon ageing was carried out. In Table 1 the initial and final characteristic values after the ageing of one of the samples are presented. The reference samples that were kept in the dark at the room temperature did show only very small changes in their I-V curves. The I-V curves in the dark and upon illumination by the blue LEDs before and after the ageing are shown in Figure 6.

Figure 7 shows the complete dynamics of the light I-V curve under ageing conditions (blue light, $\mathrm{T} = 37^\circ\mathrm{C}$). A most prominent decrease of efficiency occurs in the first hours, and the decay is not a single exponential. The short circuit current ($I_{\rm SC}$), the fill factor (FF) and the saturation ratio, defined by $I(-1\,\mathrm{V})/I_{\rm SC}$, tend to stabilize after several hundred hours. The energy conversion efficiency degrades down to less than 50% of the initial value still tending to a final non zero value. The degradation kinetics of all parameters except V_{OC} could be described well by stretched exponents as, e.g., presented by Eqs. (3), (4) for I_{SC} with different parameters:

$$I_{SC} = I_{SC0} \exp\left[\left(-\frac{t}{\tau}\right)^{\beta}\right], \tag{3}$$

$$t_{1/2} = \tau(\ln 2)^{1/\beta}, \tag{4}$$

here τ and β are parameters characterizing the stretched exponent, and $t_{1/2}$ is the half-lifetime of the relaxation. All these values are presented in Table 2 for different

Table 1. The characteristic values of the investigated cell before and after the ageing

Time (h)	V_{OC} (V)	I_{SC} (μA)	Fill factor (FF)	$I(-1\mathrm{V})/I_{SC}$	Maximum power (MP) ($\mathrm{mW/cm^2}$)
0	0.47	232	0.402	1.29	0.069
1269	0.47	154	0.232	1.57	0.027

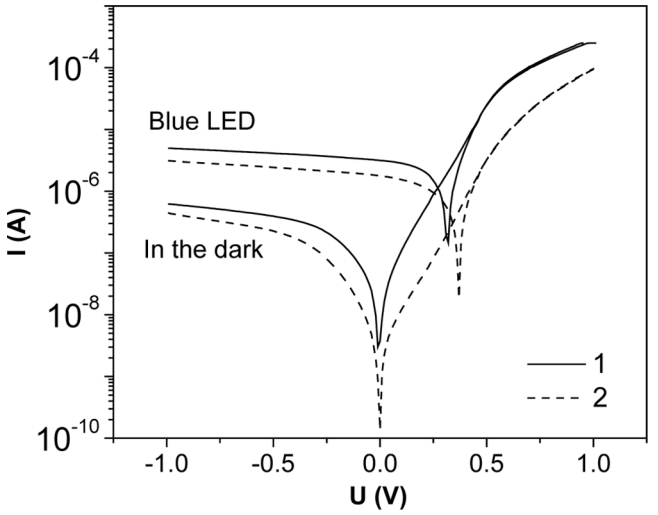

Figure 6. IV curves in the dark and upon illumination by the blue LEDs before (solid curve 1) and after the ageing (dashed curve 2).

parameters of the cells. For most of the devices V_{OC} usually remained the same or used to increase slightly, or did not change. This behaviour coincides with the behaviour of the potential barrier height described below.

3.2. *Current-Voltage (I-V) Dependencies*

To reveal properties of the interface barriers, we had measured I-Vs at different temperatures, the example of which is presented in Figure 8.

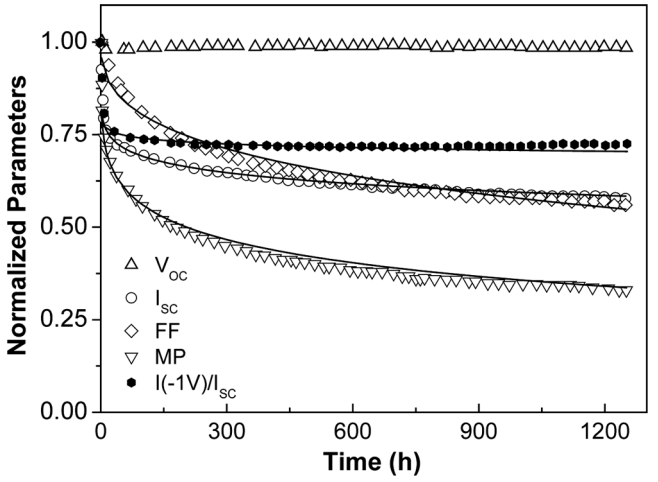

Figure 7. Variation of the characteristic parameters of the investigated structure with time upon ageing (blue light, T = 37°C). Points – experimental data, dashed curves – fittings by the stretched exponents.

Table 2. Parameters of the stretched exponents, characterizing decay of I_{SC}, FF, MP and $I(-1\,\mathrm{V})/I_{SC}$ with time

	τ (h)	β	$t_{1/2}$ (h)
I_{SC}	8×10^4	0.15	6950
FF	4500	0.4	1800
MP	900	0.25	207
$I(-1\,\mathrm{V})/I_{SC}$	5×10^{10}	0.06	1.11×10^8

To analyze the I-V characteristics we have evaluated the influence of several mechanisms that are usually accounted for in organic devices. The necessity of that is clearly evidenced by the fact that the relative increase of the reverse current exceeds that of the forward current in the same temperature region, as it is seen in Figure 8. In the forward direction up to the voltages of about 0.5 V dependence of the current is nearly exponential, afterwards the current growth becomes less expressed. In reverse direction current growth is much less pronounced and tends to saturate. Owing to the fact that conductivity of C60 is much higher than that of ZnPC, the exponential behaviour of current $I(U)$ on applied voltage U and saturation of it in reverse direction can be described by the Schottky barrier model as in [12]. This general diode equation describes the I-V characteristics of both *p-n* junctions and Schottky diodes

$$I(U) = I_s\left[\exp\left(\frac{e(U - I(U)R_s)}{nkT}\right) - 1\right], \tag{5}$$

here I_s is a saturation current, R_s is a serial resistance of the sample volume, n is the ideality factor, T is temperature, e is elementary charge, and k is Boltzmann constant. n is unity in the Shockley theory for *p-n* junctions in the absence of

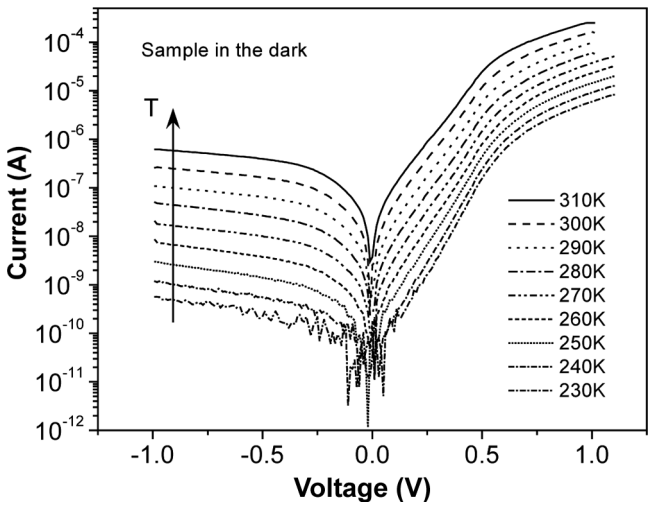

Figure 8. I-V curves of the reference sample measured in the dark at different temperatures as indicated on the Figure.

recombination, as well as for thermionic emission theory and diffusion theory for Schottky diodes. The ideality factor and the saturation current can be obtained from the slope and the intercept, respectively, obtained by extrapolation of the linear part of the semilogarithmic plot of I vs V.

The saturation current density is given by:

$$j_s = A^* T^2 \exp\left(-\frac{e\Phi_B}{kT}\right), \tag{6}$$

here A^* is the Richardson constant and Φ_B is a contact potential barrier. Therefore, using Equation 6, the contact potential barrier height can be evaluated from the temperature dependence of the reverse current. The plots of the reverse and forward current values are presented in Figure 9 for the reference and the aged samples.

It can be seen that the characteristic contact barrier is about 0.55 eV in the reference sample, similar to other evaluations, e.g., [6,13]. After degradation it grows by about 0.08 eV up to 0.63 eV. It is necessary to note that, as pointed above, V_{OC}, which is related with the potential barrier height, also slightly increases in the aged samples. Therefore one can suppose that because of degradation this barrier difference increases.

The slow growth of the reverse current with voltage could be due to the field-assisted thermionic injection over the image force barrier (Schottky effect) [14]:

$$j = AF^{3/4} \exp\left(2\sqrt{\frac{e\gamma}{kT}F}\right), \tag{7}$$

here F is the electric field strength, $\gamma = e^2/16\pi\varepsilon\varepsilon_0 kT$, and $A(F) = \text{const}$. Unfortunately this model, though explaining the field dependence of the reverse current, does not give any numerical values, characterizing the barrier.

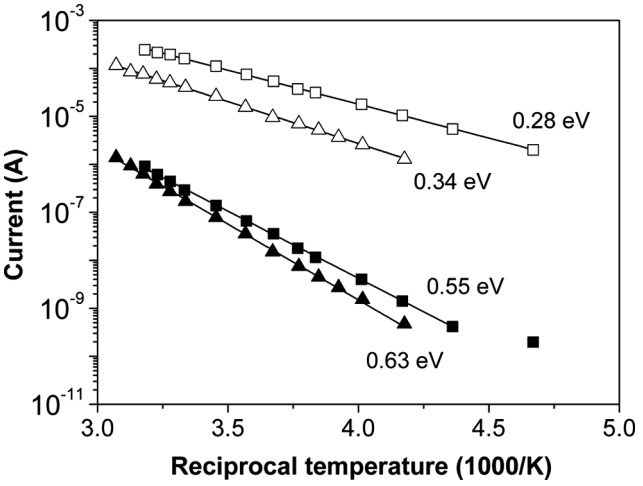

Figure 9. Dependencies of the forward and reverse current values measured at −0.9 V (filled symbols) and +0.9 V (open symbols), respectively, on the temperature in two samples: the reference (squares) and in the aged ones (triangles).

In the forward direction the exponential growth prevails up to about 0.5–0.6 V, what coincides with the height of the contact potential barrier. Above that point another current limiting mechanism starts playing a role, namely, the sample resistance R_s becomes effective. To analyse the temperature dependence of the forward current in this mode, one has to take into account also the exponential dependence of this sample volume resistance (either because of the thermal generation of carriers or their mobility variation with temperature):

$$R_s = R_{s0} \exp\left(\frac{eE_A}{kT}\right), \tag{8}$$

here E_A is the effective thermal activation energy value of sample resistance. Therefore the lower activation energy values in forward direction evaluated from Figure 9 characterize namely the thermal activation energy values of the sample conductivity. Again, slightly lower values of about 0.28 eV are characteristic for the reference sample, and they grow up to about 0.34 eV after ageing.

Other contact phenomena, limiting the current flow can be the Fowler-Nordheim tunnelling through potential barrier [15–17] or space charge limited currents [16–19] were not effective in the samples.

We have fitted the experimental dependencies, presented in Figure 8 by Eqs. (5)–(8) and a good agreement was achieved with the similar as above fitting parameters, the ideality factor n approx. equal to 3.1 and the sample resistance of about 1650 Ohms at 300 K. The ideality factor n is relatively high, but in many cases in organic structures even the best reported values exceed $2 - 2.2$ [12]. Moreover, it was found in [20] that n in ZnPc devices linearly depends on reciprocal temperature. On the other hand, in many papers factor n could be estimated to be significantly higher, though the numerical values are usually not presented.

3.3. *Carrier Mobility*

Carrier mobility dependencies on electric field strength in the reference and the aged samples at different temperatures are presented in Figure 10. Comparison of mobility behaviour at $T = 300$ K in both samples is presented in Figure 11. It can be seen that in the investigated samples the usual mobility increase with electric filed prevails in contrast to the so-called negative mobility behaviour that could be observed in highly spatially inhomogeneous materials [21,22]. To analyse mobility behaviour, we have used the Gaussian Disorder Model that is usually used for that.

Though in general, by interpreting experimental mobility results in organic and disordered materials, usually the problem arises that no theory adequately explains various transport phenomena, particularly the electric field and temperature dependencies of drift mobility [10,23–27]. The most frequently used approaches refer to hopping transport character in disordered organic solids and are based either on a modified Poole-Frenkel (PF) model [24] or a Gaussian disorder model (GDM) [28]. The latter was later extended to include correlation effects [29–31]. In the Poole-Frenkel (PF) model the mobility can be described as a field and temperature assisted detrapping process of a carrier from the Coulomb potential of a charged trap. Nevertheless this model, though being able to describe both mobility increase with electric field strength as well as its decrease, does not provide any physical clues about

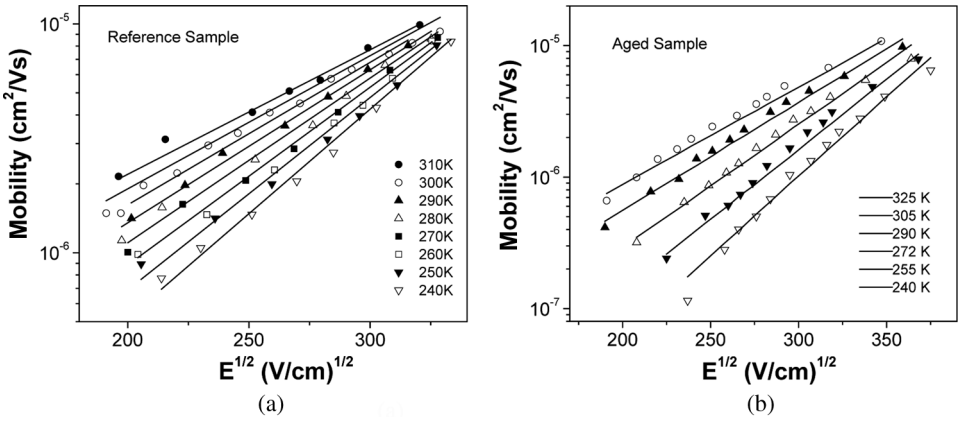

Figure 10. Carrier mobility dependencies on applied electric field strength at different temperatures as indicated on the Figures in the reference sample (a) and the aged structure (b). Lines represent fitting of the experimental data by the Gaussian Disorder Model according to Eq. (9).

the nature of the processes. In the GDM model charge transport in disordered organic conductors is supposed to proceed by means of hopping in a Gaussian site-energy distribution. This density of states (DOS) reflects the energetic spread in the charge transporting levels of chain segments due to fluctuation in conjugation lengths and structural disorder. Within the Gaussian disorder model the mobility is given by [28]:

$$\mu(F,T) = \mu_\infty \exp\left[-\left(\frac{2\sigma}{3kT}\right)^2\right] \exp\left\{C\left[\left(\frac{\sigma}{kT}\right)^2 - \Sigma^2\right]\sqrt{F}\right\}. \tag{8}$$

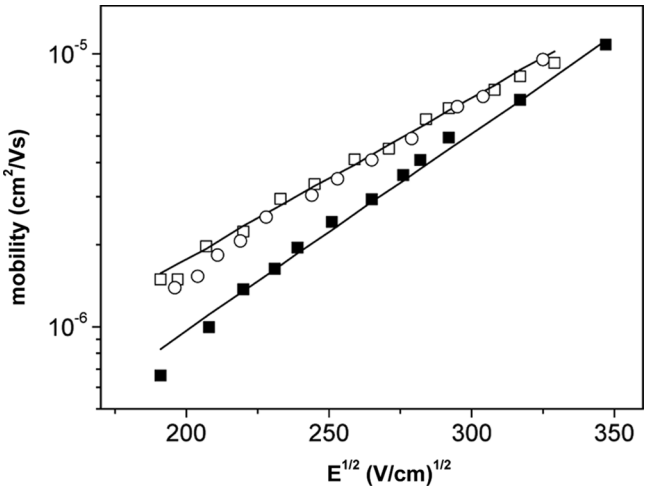

Figure 11. Carrier mobility dependencies on applied electric field strength at 300 K in the reference samples (open symbols) and the aged structure (filled squares). Lines represent fitting of the experimental data by the Gaussian Disorder Model according to Eq. (9).

Table 3. Fitting parameters of the GDM model used to fit mobility behaviour in the pristine and aged samples

	Reference sample	Aged sample
Σ	0.2	0.7
σ (eV)	0.0955	0.107
μ_∞ (cm^2/Vs)	5.00×10^{-5}	7.00×10^{-5}
C (cm/V)$^{0.5}$	1.00×10^{-3}	1.00×10^{-3}

This equation was derived from Monte-Carlo simulations of the hopping processes of charge carriers in a material with energetic (σ) and positional disorder (Σ) described be Gaussian distribution functions. μ_∞ is the high temperature limit of the mobility and C is a specific parameter that is obtained from the simulations as $C = 2.9 \times 10^{-4}$ (cm/V)$^{1/2}$. In this case a difference between the mobility decrease and increase with electric field, as implied by Eq. (8), can be attributed to the change of the influence of energetic and positional disorder. Therefore the GDM model was used to fit the experimental data as presented in Figures 10–11 by the solid lines. We have used the same fitting parameters for the single samples, just the temperature was varied. The fitting values for the pristine and the aged samples are given in Table 3.

It can be seen that distinctive increase of both energy and spatial disorder parameters occurs in the aged sample, similar to that of the values of the energy parameters obtained from the I-V measurements. Therefore one can suppose that hopping carrier transport becomes aggravated upon ageing due to increasing of both – energetic and spatial disorder of the hopping states. First of all this logically results in decrease of the sample conductivity as well as growth of its activation energy. Indeed to take part in conductivity, carriers have to move in a greater energetic and spatial disorder, meaning that their jumps between hopping states have to be energized more. Moreover, increasing material disorder leads also to the increase of the mean potential barrier height that governs carrier flow over the barrier giving the rectifying behaviour.

Summary and Conclusions

We have presented investigation of the ageing properties of ZnPc/C60 Solar cells as they are influenced by the variation of energetic parameters characterizing material conductivity, potential barrier height and charge carrier mobility. The test Solar cell structures were formed on the glass plates covered with ozone treated Indium Tin Oxide (ITO). They consisted of layers of ITO/ZnPc (18 nm)/C60 (52 nm)/AOB doped C60 (5 nm)/Al (100 nm). A ZnPc buffer was used instead of the usual phenanthroline derivatives due to its higher thermal stability, without affecting the overall device behaviour. The devices were encapsulated. The simple test device structure showed a reasonable conversion efficiency of about 1.5%.

The devices were aged for 1300 hours upon illumination with blue LED, with peak emission at 475 nm, incident light power density of 10 mW/cm^2. The devices aged under light showed a strong and fast degradation of the short circuit current and of the fill factor after several hours followed by an almost constant behaviour

of these values. The reference samples kept in the dark at the room temperature did show only very small changes in their I-V curves.

Parameters, characterizing the potential barrier height giving the diode-like behaviour and the activation energy value of material conductivity were evaluated from I-V dependencies at different temperatures. It was found that the potential barrier of about 0.55 eV evaluated in the reference sample, increased after degradation up to 0.63 eV. Meanwhile thermal activation energy values of the electrical conductivity grew from about 0.28 eV prior to degradation up to about 0.34 eV after ageing.

Carrier mobility dependencies on electric field strength at different temperatures were measured by the Charge Extraction by Linearly Increasing Voltage (CELIV) method. It was demonstrated that mobility values decrease during degradation as compared to the reference samples. These changes result from the increase of both energetic (σ) and positional disorder (Σ) parameters within the Gaussian Disorder Model. Therefore hopping carrier transport becomes aggravated, resulting in decrease of the sample conductivity as well as growth of its activation energy. This means that the jumps of the carriers between hopping states have to be energized more to move in a greater energetic and spatial disorder in order to take part in conductivity. Moreover, increasing material disorder also causes growth of the mean potential barrier height that governs carrier flow over the barrier giving the diode-like behaviour.

Acknowledgments

R. Lessmann acknowledges CAPES/Brazil and DAAD for the scholarship. Part of this work was performed within the EC FP6 project OrgaPVNet.

References

[1] Tang, C. W. (1986). *Appl. Phys. Lett.*, *48*, 183.
[2] Taima, T., Toyoshima, S., Hara, K., Saito, K., & Yase, K. (2006). *Jap. J. Appl. Phys. Part 2*, *45*, L217.
[3] Lof, R. W., van Veenandaal, M. A., Koopmans, B., Jonkman, H. T., & Sawatzky, G. A. (1992). *Phys. Rev. Lett.*, *68*(26), 3924–3927.
[4] Singh, Th. B., Marjanovic, N., Matt, G. J., Gunes, S., Sariciftci, N. S., Montaigne Ramil, A., Andreev, A., Sitter, H., Schwodiauer, R., & Bauer, S. (2005). *Org. Electron.*, *6*, 105.
[5] Pfuetzner, S., Meiss, J., Petrich, A., Leo, K., & Riede, M. in preparation.
[6] Gebeyehu, D., Maennig, B., Drechsel, J., Leo, K., & Pfeiffer, M. (2003). *Sol. Energy Mater. Sol. Cells*, *79*, 81.
[7] Green, M. A., Emery, K., Hishikawa, Y., & Warta, W. (2009). *Prog. Photovolt: Res. Appl.*, *17*, 85.
[8] Kim, J. Y., Lee, K., Coates, N. E., Moses, D., Nguyen, T. Q., Dante, M., & Heeger, A. J. (2007). *Science*, *317*, 222.
[9] Juška, G., Arlauskas, K., Viliūnas, M., Genevičius, K., Osterbacka, R., & Stubb, H. (2000). *Phys. Rev. B*, *62*, R16235.
[10] Borsenberger, P. M. & Weiss, D. S. (1998). *Organic Photoreceptors for Xerography*, Dekker: New York.
[11] Juška, G., Genevičius, K., Viliūnas, M., Arlauskas, K., Österbacka, R., & Stubb, H. (2001). *Proc. SPIE*, *4415*, 145.
[12] Riess, W. (1997). Single- and Heterolayer Polymeric Light Emitting Diodes Based on Poly(p-Phenylene Vinylene) and Oxadiazole Polymers, In: *Organic electroluminescent*

materials and devices, Miyata, S. & Nalva, H. S. (Eds.), Amsterdam: Gordon and Breach, 73–146.
[13] Egginger, M., Koeppe, R., Meghdadi, F., Troshin, P. A., Lyubovskaya, R. N., Meissner, D., & Sariciftci, N. S. (2006). *Proc. SPIE*, *6192*, 348.
[14] Godlewski, J. & Kalinowski, J. (1989). *Jap. J. Appl. Phys.*, *28*, 21.
[15] Fowler, R. H. & Nordheim, L. (1928). *Proc. R. Soc. London, Ser. A*, *119*, 173.
[16] Lampert, M. A. & Mark, P. (1970). *Current Injection in Solids*, Academic Press: New York.
[17] Sze, S. M. (1981). *Physics of Semiconductor Devices*, Wiley: New York.
[18] Pope, M. & Svenberg, C. E. (1982). *Electronic Processes in Organic Semicondutors*, Oxford University Press: New York.
[19] Mott, N. F. & Gurney, R. W. (1940). *Electronic Processes in Ionic Crystals*, Oxford University Press: New York.
[20] Harada, K., Werner, A. G., Pfeiffer, M., Bloom, C. J., Elliott, C. M., & Leo, K. (2005). *Phys. Rev. Lett.*, *94*, 036601.
[21] Mozer, A. J., Sariciftci, N. S., Pivrikas, A., Österbacka, R., Juška, G., Brassat, L., & Bässler, H. (2005). *Phys. Rev. B*, *71*, 035214.
[22] Kažukauskas, V., Pranaitis, M., Sicot, L., & Kajzar, F. (2006). *Mol. Cryst. Liq. Cryst.*, *447*, 459.
[23] Kepler, R. G., Beeson, P. M., Jacobs, S. J., Anderson, R. A., Sinclair, M. B., Valencia, V. S., & Cahill, P. A. (1995). *Appl. Phys. Lett.*, *66*, 3618.
[24] Gill, W. D. (1972). *Appl. Phys.*, *43*, 5033.
[25] Abkowitz, M. A. (1992). *Philos. Mag. B*, *65*, 817.
[26] Schein, L. B. (1992). *Philos. Mag. B*, *65*, 795.
[27] Blom, P. W. M. & Vissenberg, M. C. J. M. (2000). *Mater. Sci. Eng.*, *27*, 53.
[28] Baessler, H. (1993). *Phys. Stat. Solidi (b)*, *175*, 15.
[29] Dunlap, D. H., Parris, P. E., & Kenkre, V. M. (1996). *Phys. Rev. Lett.*, *77*, 542.
[30] Novikov, S. V., Dunlap, D. H., Kenkre, V. M., Parris, P. E., & Vannikov, A. V. (1998). *Phys Rev. Let.*, *81*, 4472.
[31] Dunlap, D. H., Kenkre, V. M., & Parris, P. E. (1999). *J. Imag. Sci. Technol.*, *43*, 437.